Journal of the Korean Ceramic Society
Vol. 30, No. 12 PP. 1089~1095, 1993.

Structure of the α-Al_2O_3 $(1\bar{1}00)$ Surfaces

Yootaek Kim, Kigang Lee and Dong-Won Kim
Department of Materials Engineering, College of Engineering, Kyonggi University
(Received October 5, 1993)

알파 알루미나 $(1\bar{1}00)$ 표면의 구조

김유택 · 이기강 · 김동원
경기대학교 공과대학 재료공학과
(1993년 10월 5일 접수)

ABSTRACT

The α-Al_2O_3 $(1\bar{1}00)$ surfaces were studied with reflection electron microscopy (REM) technique. Severely faceted surfaces were found in the $\langle 11\bar{2}0\rangle$ azimuth. Two methods were applied for indexing the facets. The facets are indexed as $(1\bar{1}0\bar{1})$ and vicinal facets of $(1\bar{1}02)$, while the macroscopic plane is $(1\bar{1}00)$.

요 약

반사전자현미경법을 이용하여 알파 알루미나 $(1\bar{1}00)$표면을 관찰하였다. $\langle 11\bar{2}0\rangle$방위에서 $(1\bar{1}00)$표면을 관찰한 결과 매우 심한 facet들로 이루어진 표면이 관찰되었다. 이들의 면지수를 결정하는데 두가지 방법이 사용되어 비교, 검토되었다. 결과적으로 거시적인 결정면은 $(1\bar{1}00)$면이었으나, facet들의 면지수는 $(1\bar{1}0\bar{1})$면과 $(1\bar{1}02)$면을 포함한 주변의 면들로 판명되었다.

1. Introduction

In recent years, several low index surfaces of α-Al_2O_3 have been studied with the conventional transmission electron microscopy (CTEM)[1], high resolution TEM (HRTEM)[2], and low energy electron diffraction (LEED) methods[3]. The $(1\bar{1}00)$ surface is one of the prismatic faces ($\{10\bar{1}0\}$ and $\{11\bar{2}0\}$). TEM study revealed that there are several facts on these surfaces[1]. However, there are some of the disadvantages of TEM for indexing the surface facets. Recently, these prismatic faces have been studied with reflection electron microscopy (REM) and have some domains on them[4]. Kim et al.[5] also presented severely faceted $(1\bar{1}00)$ surface with comparisons of other orientation surfaces.

In this study, the combined reflection high energy electron diffraction (RHEED) and REM techniques are applied for indexing the facets on the α-Al_2O_3 $(1\bar{1}00)$ surfaces.

2. Experimental

Alpha-Al_2O_3 specimens were manufactured with the edge-defined film-fed growth (EFG) method by Saphikon, Inc., Milford, NH. Specimen orientation was confirmed using the Laue X-ray diffraction camera. Fig. 1 shows a Laue back-reflection pattern of the $(1\bar{1}00)$ surface. This pattern indicates that the macroscopic orientation of the surface is exactly $(1\bar{1}00)$. The specimens were mechanically polished, then annealed at 1400℃ for 24 hours in air. Details of the specimen preparation procedure has been reported elsewhere[6]. The REM observations were done in JEM-200CX and JEM-2000 EX electron microscopes.

3. Results and Discussion

3.1. Surface Morphology

3.1 1. The as-grown/polished $(1\bar{1}00)$ surface

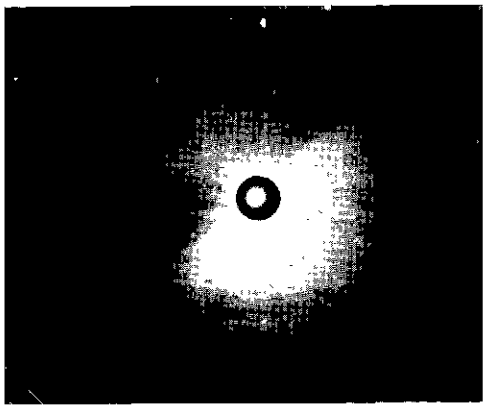

Fig. 1. Back-reflection Laue patterns of the $(1\bar{1}00)$ surfaces.

Alpha-Al_2O_3 ribbons which had been drawn by EFG method in the $[1\bar{1}00]$ direction were cut to various lengths in a way that the $(1\bar{1}00)$ surface is the cut surface.

The width of $(1\bar{1}00)$ face on the as-grown ribbons is less than 2mm wide. Their corners are rounded so that very small flat areas can be examined. The as-grown $(1\bar{1}00)$ surfaces are very rough, so that it was not successful in obtaining any useful RHEED patterns and REM images from these surfaces. Even after polishing, these surfaces did not deliver any sharp RHEED patterns. Our trial has suggested that these as-grown and polished surfaces are not suitable for RHEED or REM analysis.

3.1.2. The annealed $(1\bar{1}00)$ surfaces

The regularly faceted surface configuration was found on the annealed $(1\bar{1}00)$ surfaces in the $[11\bar{2}0]$ azimuth. No regularly faceted surface was found in the [0001] azimuth. Fig. 2a and 2b show typical surface morphologies of the annealed $(1\bar{1}00)$ surfaces in the $[11\bar{2}0]$ and [0001] azimuths, respectively. Note that in Fig. 2a there are two types of facets. One is atomically flat (F-facet) and another is rough and curved (R-facet). Atomic steps indicated by arrows in Fig. 2a are presented on F-facets. The distribution of F-facets and R-facets is relatively uniform throughout the specimen.

3.2. The Split RHEED Spots

The RHEED pattern of the annealed $(1\bar{1}00)$ surface in the $[11\bar{2}0]$ azimuth (Fig. 2a) is shown in Fig. 3. The inset shows the spots used for imaging taken at a lar-

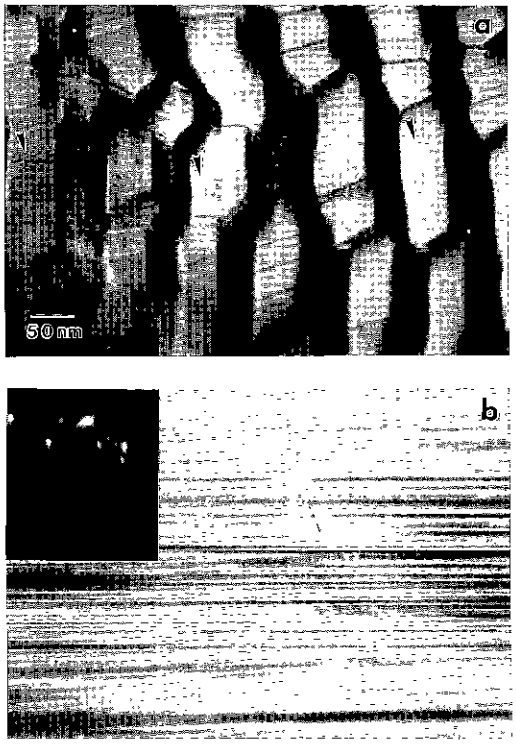

Fig. 2. Typical surface morphologies of the annealed $(1\bar{1}00)$ surfaces. (a) in the $[11\bar{2}0]$ azimuth. (d) in the [0001] azimuth. The spot at the pointer in the inset is used for producing the image of (b).

ger camera length (166 cm). There are one weak spot on the left and another strong spot on the right in the inset. The split spots indicate that the contrast of the two types of facets on the annealed $(1\bar{1}00)$ surface can be reversed by translating the objective aperture. In fact, the F-facets could be selectively illuminated by choosing a strong reflection spot (Fig. 4a), whereas the R-facets could be illuminated by choosing a weak reflection spot (Fig. 4b) If both spots are used for imaging, both facets are illminated as in Fig. 4c.

Fig. 5 shows how electron beams are reflected and refracted into slightly different directions by the faceted surfaces of the $(1\bar{1}00)$ plane. The angle between the split beams depends on the angle between the two facets, when other parameters such as wavelength and inner potential are held constant. In this case, the angle between the F- and the R-facets is about 50° (to be discussed later), which is much greater than the angle between the $(11\bar{2}0)$ and $(22\bar{4}3)$ facets[6,7]. The

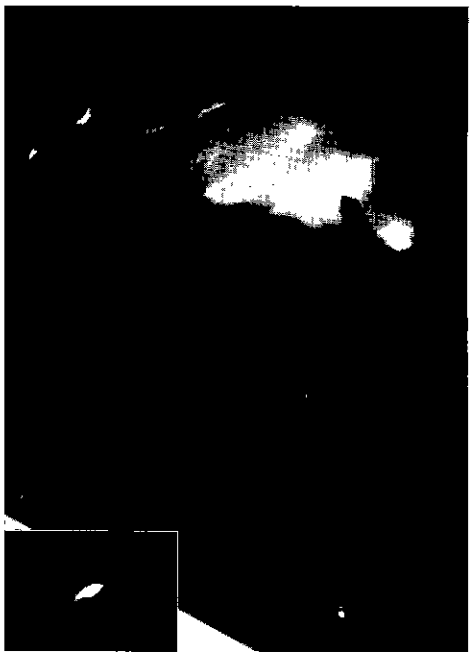

Fig. 3. The corresponding RHEED pattern of Fig. 2a. The inset shows spot splitting at a 166 cm camera length.

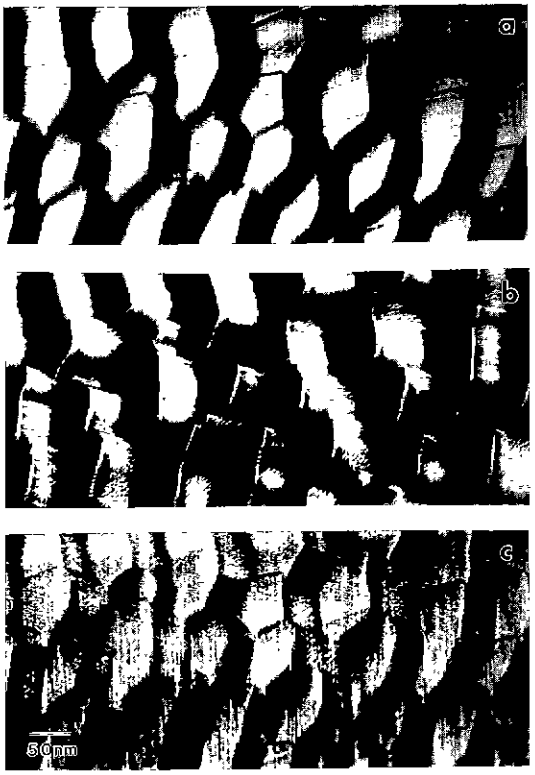

Fig. 4. A series of images from the same area shows contrast reversal of the two types of facets. (a) Only F-facets are illuminated by choosing the strong reflection spot in Fig. 3 (b) R-facets are illuminated by choosing the weak reflection spot in Fig. 3. (c) Both facets are equally illuminated by choosing both spots in Fig. 3.

weak spot on the left and strong spot on the right in Fig. 3 were related to R- and F-facets, respectively. The weak intensity of the left spot from R-facets could be caused by their surface roughness. Because there are more diffuse scattered electrons from a rough surface, the intensity of the Bragg reflected beams from a rough surface would be weaker than ones from a smooth surface.

3.3. Specular spot

Fig. 6a and 6b show REM images of two pairs of a foreign object and its inverted shadow on the $(1\bar{1}00)$ surface at different diffraction conditions. These pairs of images are usually used for determining whether the spot used for image is specular or not on the atomically flat surfaces[8,9]. If they are related by two-fold symmetry along the horizontal line, the spot is specular. If the spot used for image is not specular, the shadow image will be slanted to one side with respect to a vertical line of the image (Fig. 6b).

As shown in Fig. 6a a pair of images are not exactly symmetrical, although the shadow is not slanted at all. This asymmetry comes from the different ridge shapes of shadow. This ridge shape difference between the foreign object and shadow is likely caused by severe surface undulation of facets. When macroscopic surface is slightly tilted about the axis perpendicular to the beam direction, the shadow image can be either elongated or shortened in the beam direction, depending on the sense of tilting.

From Fig. 6a, the area in shadow is not likely tilted. If any, the possible tilt may be ignorable because the vertical length of foreign object and shadow is almost same except some areas. For comparison, the shadow image in Fig. 6b is not only slanted to the one side but also very much elongated. Therefore, it is speculated that asymmetry of Fig. 6a comes from the severely faceted surface configuration and the spot used for image is specular.

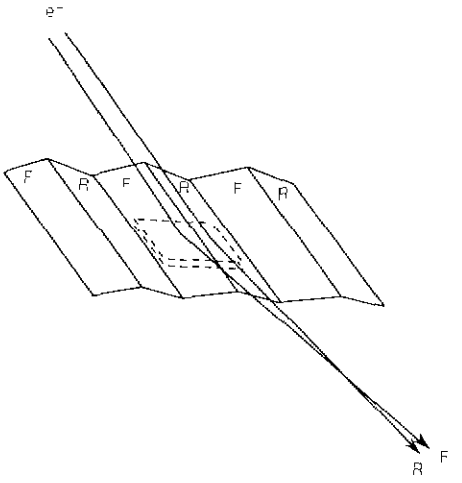

Fig. 5. A schematic diagram of electron paths at the faceted surfaces. Electrons are reflected by the atomic planes (dashed parallelograms) of the single crystal, but the faceted surface configuration refracts the beams into two different directions.

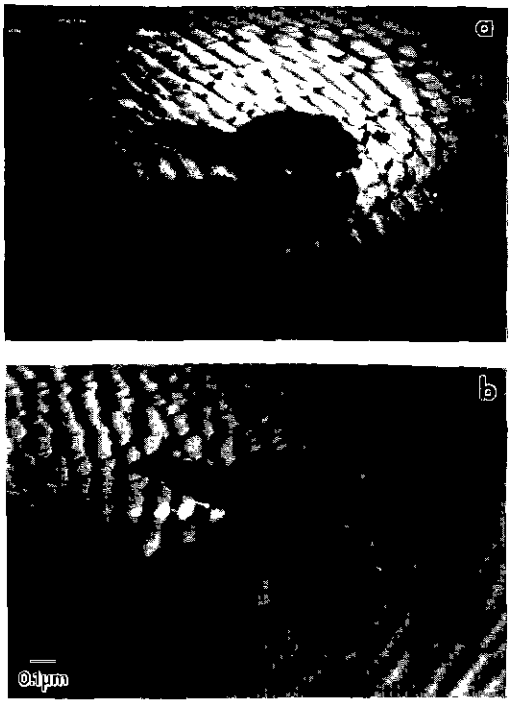

Fig. 6. REM images of two pairs of a foreign object and its inverted shadow on the $(1\bar{1}00)$ surface with different diffraction conditions. (a) when specular $[n\bar{n}00]$ beam was used for imaging. (b) when non-specular beam was used for imaging.

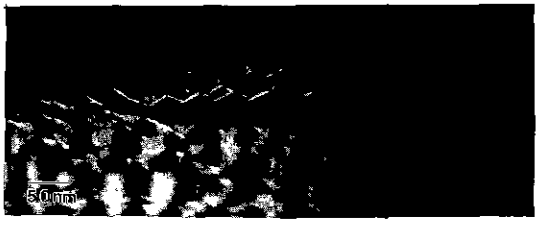

Fig. 7. The near profile image of the $(1\bar{1}00)$ surface formed by a large step. The average measured angle between two facets is 50°.

3.4. Indexing of Facets

There are several ways of indexing the facets. In this study, two methods were considered: 1) by estimated angles from REM images, and 2) by information in RHEED, transmission electron diffraction (TED), and Kikuchi patterns. Both methods were discussed and compared as follows.

3.4.1. Estimated angles from the REM images

Before indexing the facet, the index of the macro-surface could be determined adopting one of the following ways:

i) Using a back-reflection Laue camera.

ii) When transmission electron diffraction (TED) patterns are obtained from the specimen corners, the index of **g** (the diffraction vector) can be determined. From the RHEED pattern, the angle **g** and specimen shadow edge can be measured. The index of the macro-surface is the index of **g**, if **g** is perpendicular to the shadow edge[6,9].

iii) From the symmetry of the Kikuchi pattern, the index of the macro-surface can be determined.

iv) Any parallel set of Kikuchi lines can be indexed from the line spacing. If **g** is perpendicular to these Kikuchi lines, then the index of the macro-surface is the same as the index of the kikuchi lines

v) If the erect/inverted images of a foreign object on the surface is not skewed, then **g** is parallel to the surface normal. Consequently, the index of the macro-surface and the index of **g** are the same[9-11].

Once the index of the macro-surface is determined, the angle between the two facets should be measured

and averaged from the REM images.

In this study, the angle between F-and R-facets is estimated from the near profile REM images of these facets as shown in Fig. 7. The average measured angle between F-and R-facets is about 50°. The angle between the F-facet and $(1\bar{1}00)$ is $\approx 18°$, and between the R-facet and $(1\bar{1}00)$ the angle is $\approx 32°$. Accordingly, the corresponding indices of F- and R-facets are $(1\bar{1}0\bar{1})$ and $(1\bar{1}02)$, respectively.

3.4.2. By RHEED, TED, and Kikuchi patterns

The index of facets as well as the index of the macro-surface can be directly determined by RHEED, TED, and Kikuchi patterns as follows:

i) The index of **g** can be determined by a TED pattern obtainable from the sharp edge of the bulk crystal. The angular relationship between **g** and **n** (the surface normal vector) can be obtained from the erect/inverted foreign object images. Using this information as well as the symmetry of the Kikuchi pattern, a facet can be indexed.

ii) Kikuchi lines can be indexed from the line spacing. Facets can be indexed by the angular relationship between **g** and the Kikuchi lines. The angles between Kikuchi lines from different {hkl} planes correspond to the angles between the planes because the Kikuchi lines are parallel to the traces of the planes[12].

Fig. 8a, 8b, and 8c show a RHEED pattern, a schematic drawing of Fig. 8a, and the corresponding REM image, respectively. The angles between Kikuchi lines in Fig. 8a are used to obtain the angles between the crystal's reflecting planes.

The index of the spot used for imaging is $9\bar{9}00$. The indices of Kikuchi lines perpendicular to **g** (indicated by large arrows) are $n\times 1\bar{1}00$ and the line spacing corresponds to 1/2 $d_{1\bar{1}00}$ which is 0.1374 nm. The indices of Kikuchi lines indicated by small arrows are $n\times 1\bar{1}02$ and the line spacing corresponds to $d_{1\bar{1}02}$ (0.3479 nm). The angle between $1\bar{1}00$ and $1\bar{1}02$ Kikuchi lines is 32.5°. The indices of Kikuchi lines indicated by medium arrows are $1\bar{1}0\bar{1}$ and the line spacing corresponds to $d_{1\bar{1}0\bar{1}}$ (0.393 nm). The angle between $1\bar{1}00$ and $1\bar{1}0\bar{1}$ Kikuchi lines is 17.5° and between $1\bar{1}0\bar{1}$ and $1\bar{1}02$ is 50°.

As expected from an angular relationship between the Kikuchi lines in Fig. 8a and 8b, the $(1\bar{1}02)$ and $(1\bar{1}0\bar{1})$ facets make angles of 32.5° and 17.5°, respectively, with respect to the $(1\bar{1}00)$ surface.

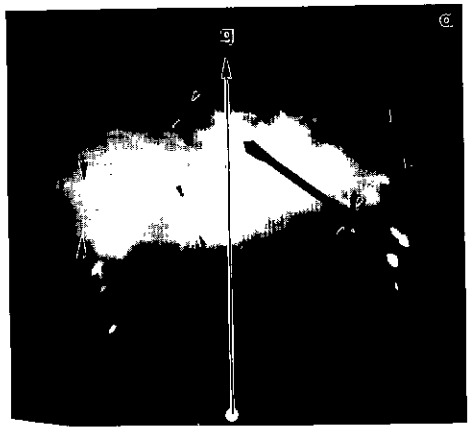

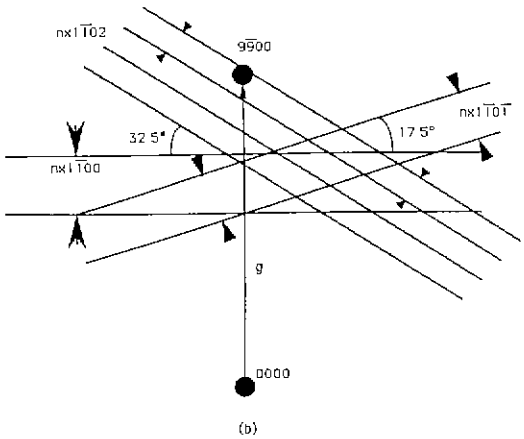

(b)

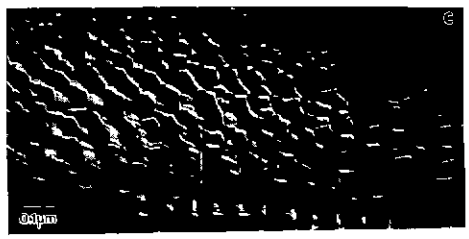

Fig. 8. A facet can be indexed from the angular relationship between Kikuchi lines. (a) A RHEED pattern. The small, medium, and large arrows indicate $1\bar{1}02$, $1\bar{1}0\bar{1}$, and $1\bar{1}00$ Kikuchi lines, respectively. (b) A schematic drawing of the Fig. 8 a. (c) The corresponding REM image.

Accordingly, the F- and R-facets are indexed as $(1\bar{1}0\bar{1})$ and $(1\bar{1}02)$. The result from this method is well matched with the previous one.

The indexing methods are summarized in the flow

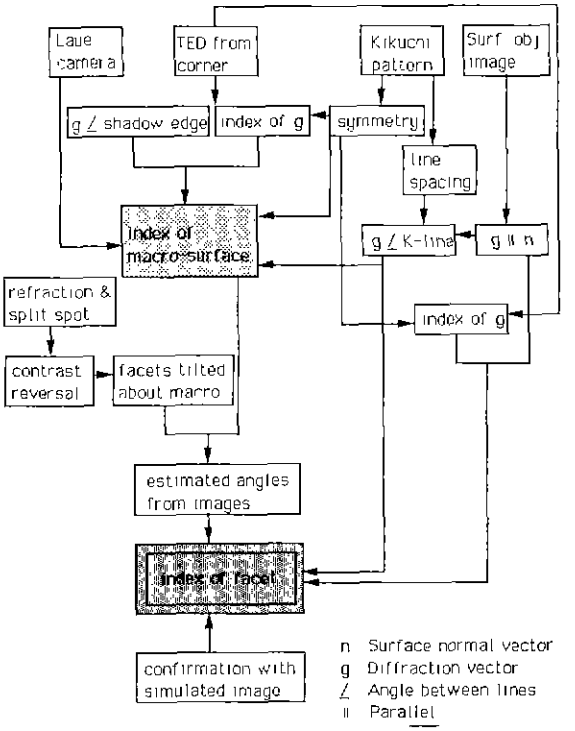

Fig. 9. The flow chart of indexing a macro-surface and a facet.

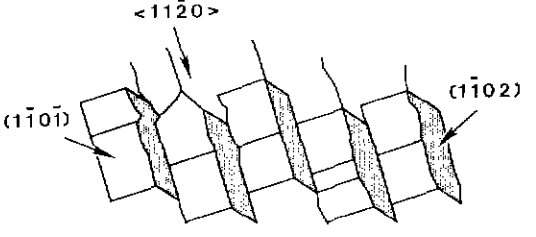

Fig. 10. Simulated facet configuration on a (1$\bar{1}$00) surface. α=4.6° and A=2.6° from [11$\bar{2}$0] where α and A are incident and azimuthal angles, respectively.

chart of Fig. 9. All of the paths in the flow chart are checked and the results are consistent.

3.4.3. Computer simulation

A computer simulated image helps to confirm the indices of facets[6]. An alternative arrangement of (1$\bar{1}$01) and (1$\bar{1}$02) and vicinal facets was constructed with (1$\bar{1}$00) surface parallel to the horizontal line. The model was then rotated by an azimuthal angle of 2.6° and the incident angle was obtained from the corresponding RHEED pattern. Fig. 10 shows the simulated facet configuration of the corresponding Figs. 2a, 4c, and 8c.

Table 1. Surface Energies of Low-Index Surfaces

Surface	Unrelaxed surface energy (j·m^{-2})		Relaxed surface energy (j·m^{-2})	
	From 13)	From 14)	From 13)	From 14)
(0001)	6.53	5.95	2.97	2.03
(1$\bar{1}$01)	6.41	5.58	3.27	2.52
(1$\bar{1}$02)	3.55	3.63	2.57	2.29
(11$\bar{2}$0)	5.17	4.37	2.65	2.50
(1$\bar{1}$00)	6.87	6.46	2.89	2.23

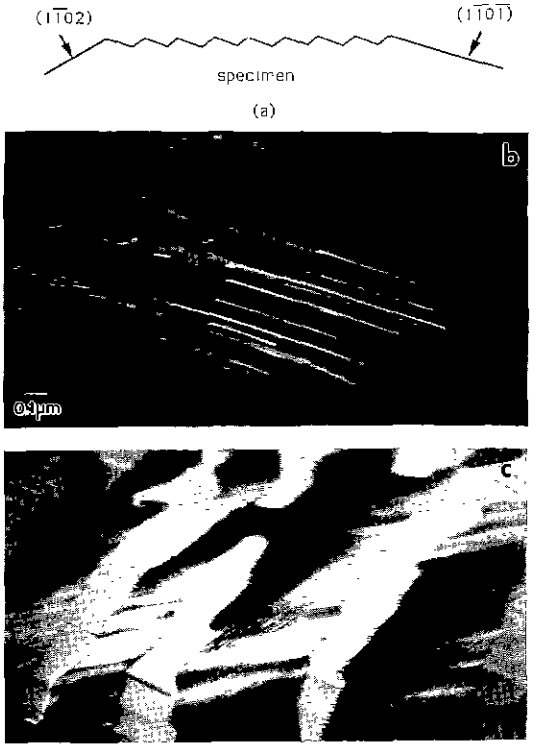

Fig. 11. The (1$\bar{1}$01) and (1$\bar{1}$02) facets observed at each end of the specimen are larger than the corresponding facets within the specimen. The facet positions were reversed with respect to those in Fig. 2a and 4c because the specimen was rotated 180° about the [1$\bar{1}$00] axis. (a) A schematic drawing of an edge-on view of the specimen surface. (b) Large (1$\bar{1}$01) facets are at one end. (c) Large (1$\bar{1}$02) facets are at the other end.

Note that the lines in the middle of the F-facets represent the atomic steps on the ($1\bar{1}0\bar{1}$) surface and the most preferred step direction is $\langle 1\bar{1}02\rangle$. Also note that the edges where ($1\bar{1}0\bar{1}$) and ($1\bar{1}02$) meet in Figs. 2a, 4, 8c and 10 are not always straight. This indicates that F-facets are ($1\bar{1}0\bar{1}$), however, R-facets are not only made of ($1\bar{1}02$) facets but also of several ($1\bar{1}02$) vicinal facets which have the same zone axis of $\langle\bar{1}101\rangle$.

Table 1 shows the calculated surface energies for the low-index surfaces from two different sources[13,14]. Here, unrelaxed and relaxed mean the states before and after equilibrium[14]. The values from the two sources are slightly different; however, the unrelaxed surface energies of both ($1\bar{1}0\bar{1}$) and ($1\bar{1}02$) are lower than that of ($1\bar{1}00$). Annealing at 1400℃ (m.p. 2076~2057℃) in air did not promote equilibrium conditions for the crystal surface. Therefore, the unrelaxed surface energies must be important and development of facets with a lower energy might be favored over the formation of the flat ($1\bar{1}00$) facet.

Large ($1\bar{1}0\bar{1}$) facets are expected to develop at one edge and ($1\bar{1}02$) and its vicinal facets at the other, as shown in Fig. 11a. To reveal these large facets, specimen edges are repolished with a certain angle with respect to the ($1\bar{1}00$) surface and then annealed. After this procedure, large facets could be observed on both edges. The large ($1\bar{1}0\bar{1}$) facets are shown in Fig. 11b and the large ($1\bar{1}02$) and its vicinal facets in Fig. 11c. In these figures, the positions of F-facets and R-facets are reversed with respect to the those in the previous figures (Figs. 2a, 4c, and 8c) because the specimen is rotated 180° about the $\langle 1\bar{1}00\rangle$.

4. Conclousion

Severely faceted surfaces were found on α-Al_2O_3 ($1\bar{1}$ 00) in the $\langle 11\bar{2}0\rangle$ azimuth, while the macroscopic plane is ($1\bar{1}00$). The facets are indexed as ($1\bar{1}0\bar{1}$) and vicinal facets of ($1\bar{1}02$) based on REM images and diffraction patterns.

Beam splitting due to the electron refraction at the crystal surface was apparently observed. The contrast of two types of facets can be reversed by translating the objective aperture.

We suggested two methods to index facets by the direct measurement of REM images and by the analysis of RHEED, TED, and Kikuchi patterns.

Acknowledgement

Part of this work is supported by the Korea SanHak Foundation. Author (YTK) thanks Lim in EM lab at Han Yang University for the help on microscope.

REFERENCES

1. D.W. Susnitzky, Y. Kouh Simpson, B.C. DeCooman, and C.B. Carter, in: Materials Res. Soc. Symp. Proc., **60**, 137 (1986).
2. L.A. Bursill, Peng Ju Lin, and D.J. Smith, Ultramicroscopy, **23**. 223 (1987).
3. J.M. Charig and D.K. Skinner, in: The Structure and Chemistry of Solid Surfaces, Ed. G. A. Somorjai, 34 (John-Wiley & Sons, New York, 1969).
4. G.C. Ndubuisi, J. Liu and J.M. Cowley, Electron Microscopy 1990, Proc. of XIIth International Congress For Electron Microscopy, **1**, 330 (1990).
5. Yootaek Kim, Microscopy 1990, Proc. of XIIth International Congress For Electron Microscopy, **1**, 328 (1990).
6. T. Hsu and Y. Kim, Ultramicroscopy, **32**, 103 (1990).
7. Y. Kim, Tung Hsu. Surface Sci., **258**, 119 (1991).
8. T. Hsu, S. Iijima, and J.M. Cowley, Surface Sci., **137**, 551 (1984).
9. T. Hsu, Phd Dissertation at Arizona State University, pp.5-8 (1983).
10. T. Hsu, and Sumio Iijima, in: Elctron Microscopy, Ed. The Congress Organizing Commiltee, Vol 2, 301 (Deutsche Gessellschaft f. Elektronenmikroskopie eV, Frankfryt, 1982).
11. K Kambe, Ultramicroscopy, **25**, 259 (1988).
12. J. W. Edington, Practical Electron Microscopy in Materials Science, pp. 50-55 (Van Nostrand Reinhold Company, NY, 1976).
13. P. W. Tasker, in. Advances in Ceramic, Vol. 10, Structure and Properties of MgO and Al_2O_3 Ceramics, Ed. W.D. Kingery, pp. 176-185 (The American Ceramic Society, Inc. Columbus, OH, 1986).
14. Surfaces and Interfaces of Ceramic Materials, Ed. L.-C Dufour, C.Monty and G. Petot-Ervas, NATO ASI series E, **173**, 185 (1988).